Transactions of the **14th International Conference on Structural Mechanics in Reactor Technology** (SMiRT 14), Lyon, France, August 17-22, 1997 **K03/5**

Shaking table tests on a real-size pile foundation in liquefying sand

Kagawa T.(1), Abe A.(2), Sakai K.(3), Ogawa N.(4), Minowa C.(4)
(1) WSU, Japan
(2) Tokyo Soil Research Co., LTD, Japan
(3) Kiso-Jiban Consultants Corporation, Japan
(4) National Research Institute for Earth Science and Disaster Prevention, Japan

ABSTRACT

This paper highlights results and analyses of a series of shaking-table tests on real-size pile foundation system in loose saturated sand. The ultimate objective of this research is to develop numerical methods and design guidelines for pile foundation in potentially liquefiable sand deposits. This study demonstrated the significance of liquefaction on pile responses and provided an improved understanding of the soil-pile interaction in liquefying sand.

1 . INTRODUCTION

Piles increase the performance of foundations at potentially liquefiable sites. This has been evidenced in various disastrous earthquakes. At the same time, a number of pile foundations have been found damaged and failed during major historical earthquakes; Kobe earthquake. This is partly because the state of the art in this field has not advanced to a point where we can predict the performance of pile foundations when the surrounding soils undergo liquefaction during an earthquake.

In 1996, National Research Center for Earth Science and Disaster Prevention (NIED) developed a large-scale laminar shear box which has 6m in height, 12m in length, 3.5m in width. The laminar shear box was designed to deform more than 1m in one horizontal direction. The wall of large-scale laminar shear box was composed with 30 laminar unit of 20cm height. The box which set on one horizontal large-scale shaking table of NIED was used.

The paper highlights the first shaking table test on real-size pile foundation in loose saturated sand. This is followed by results from our numerical analyses using existing nonlinear soil-pile-structure interaction methods.

2 DESCRIPTION OF SHAKING TABLE TESTS AND LARGE-SCALE LAMINAR SHEAR BOX

2.1 Background

Field observational data on the earthquake response of pile foundations in liquefying sand layers are very scarce at present. Therefore, this study attempts to establish reliable experimental data on the responses of piles when surrounding soils undergo liquefaction. Such data may be obtained by two key experimental methods, centrifuge tests and 1-g model test. The similitude

requirements for these types of tests were summarized by several investigation; e.g., Kagawa(1978). Centrifuge tests involve large geometric scaling, typically on the order of 50 to 100. Therefore, it becomes difficult to satisfy the geometrical similarity on the sizes of soil particles and shear bands. These, in addition to some other factors, may result in incorrect representation of the failure strength of the sand mass around the model pile. Also small-scale tests require large reduction in the rate of pore pressure redistribution. For these reasons, the authors prefer 1-g model tests with reasonably large models.This is the reason of the need of large-scale shaking table and laminar shear box.

2.2 Shaking table and laminar shear box

The one horizontal shaking table belongs to NIED. The peak velocity performance of the table has been improved to 100cm/sec from 75cm/sec in 1996. The table has the dimension of 12m by 12m, the maximum displacement of 23cm, the weight of 180ton, the maximum power of 360tonf, and the maximum test weight 500ton approximately.

The large-scale laminar shear box was assembled on the shaking table. The movements of laminar units of box was limited in one horizontal direction by 6 guide frames. The total weight of the shear box with guide frames was about 110ton. The box and guide frame weights were estimated to be 50ton and 60ton respectively. The roller bearing of 20cm diameter were installed between adjacent laminar units which were made of H-steel. The inner side gaps between laminar units were filled with Teflon plates. The limit relative displacements between each laminar unit was 10cm. The inside of laminar shear box was sealed with expanding rubber sheet.

2.3 The performance tests of large-scale laminar shear box.

In order to measure the friction between laminar units, the empty large-scale laminar shear box was excited in 1Hz. The upper laminar unit slipped at the amplitude of 20gal. The bottom laminar unit slipped at 70gal. The test weight capacity of the box was about 400ton. The weight ratio of box and test layer was 1/8.

The slip excitation tried so as to make a large residual deformation in the box. The input waves which was measured in the shaking table, show in Fig.1. Considering the friction resistance, the acceleration of input waves provided the one side large amplitude. 20 peak accelerations were given to the box. The amplitude ratio of two sides was 1/5. The residual deformation was about 60cm, as shown in Fig.2.

2.4 Liquefying reaction to actuators

In order to control the actuators, oil pressure sensors were installed. Using the sensors, actuating force F was estimated. The actuating force would be expressed using the rigid table mass m_0, test structure mass m_t, the table acceleration $\ddot{y}$, and test structure acceleration $\ddot{x}$, as follows.

$$F = m_0\ddot{y} + m_t\ddot{x} \qquad (1)$$

In this test, m_0 was 290ton. According to the expression and records F, the reaction force from liquefying test structure would be estimated. Furthermore, the works which the actuators made for the liquefying sand layer would be estimated with the time integral of the following expression,

$$(F - m_0\ddot{y}) \times \dot{y} \qquad (2)$$

In Fig. 3 and 4, the sample records were shown. The excess pore pressure records

of saturated sand layer was first line in the figures. The whole sand liquefaction points would be something corresponding to shaking table works.

2.5 Sand Layer

The saturated sand layers for the tests were prepared in a laminar shear box with an inner plan dimension of 11.6 by 3.1 meter and a height of 6 meter. The test sand was the Hokota sand taken from northern part of Kasumigaura Lake near the city of Tsukuba,Japan. The percent weight of fines(slit and clays) was 5.4%; the particle diameter (D_{50}) was 0.311cm; the maximum and minimum dry densities were 1.73 and 1.39 g/cm^3; and the natural water content was 5.7%.

A fresh sand layer was prepared by pouring the wet test sand into the shear box, partially filled with water. The relative density of sand layer thus prepared was about 48.8%; the estimate void ratio was about 0.770; and the shear wave velocity of the sand layer was about 135 m/sec.

2.6 Test Pile Foundation

The test pile foundation system consisted of two "Prestressed High Strength Concrete" (PHC) piles, two "Prestressed and Reinforced Concrete"(PRC) piles, placed in center of shear box with distance of 1.8m and a steel mass of weight 22.5ton. The length ,diameter, ans the thickness of four piles were 6m and 30cm, and 10cm. The plan dimension of the steel mass was 2.5m by 2.5m with a height of 45cm. The steel mass represented a structure with a translational degree-of-freedom only. Four pile were fixed into cylindrical holes of the steel mass with mortar, to provide the rotational constraint to the test piles. The tips of four test piles were pinned at the base of the shear box. Therefore, they were free to rotate. The equivalent geometrical moment of inertia, design damage bending moments and shear forces for piles were 36306 cm^4, 7.17ton, 12.9 for PHC piles, and 40602 cm^4 10.41ton, 12.1ton for PRC piles. PRC piles were a little bit stronger than PHC piles. Fig. 5 shows a schematic views of test sand layer and pile systems.

2.7 Instrumentation

For the sand layer, acceleration response were measured at 12 levels, and excess pore-water pressures were measured also at 12 levels at two positions near pile system in the use of expanding plastic grid columns.

For the test pile foundation system, strain gages were attached to the reinforcement steel bars embedded in one PHC pile and one PRC pile. Acceleration and excess pore pressure responses of one PHC pile were measured at 11 levels corresponding to sand layer measurement levels.

2.8 Shaking-Table Input

Pile foundation system was excited four times. First input was Kobe Port-island -32m NS component of times scale 1/2 and amplitude 350gal. Second one was sweep excitation of 50gal. Third one was same wave to first one. However, time scale was 1/1 and the amplitude was 600gal. Fourth input was JMA Kobe NS component of 100kine.

3 SUMMARY OF TEST RESULTS

The water proof video camera was used for pile integrity tests. No remarkable cracks were found in first and second inputs. In third and fourth excitations, the pile cracks were produced. After the sand layer was removed, the pile cracks were observed and sketched. The cracks distributed all over the pile surfaces

from bottoms to tops. Main cracks concentrated in upper positions near steel mass. Comparing the cracks of PHC and PRC piles, the cracks of PHC piles were count much more and grew larger. The crack intervals and extensions of FRC piles were almost same. The photo and sketch of pile cracks were shown in Fig. 6 and 7.

4 NUMERICAL ANALYSIS METHODS

Response of the test pile-foundation system to a shaking table excitation was computed in two steps; computation of the response of sand layer and computation of response of the test piles. Key feature of the numerical methods used in this study are highlighted by Kagawa (1992).

It was reasonable to assume that the sand layer in the laminar shear box deformed in one-dimensional shear. Therefore. The response of the sand layer was obtained by SRANG that is based on the one-dimensional wave propagation theory. Computed responses of the sand layer were then used, as multiple soil-support input motions, in a subsequent soil-pile-structure interaction analysis by NONSPS. The stress-strain relation of the sand was represented by a multiple, elastic-plastic spring model, which may be considered a simple version of multi-surface plasticity model. Excess pore pressure developed in the sand layers during shaking and they redistributed during and after shaking. The simple pore pressure model(Kagawa and Kraft, 1981) was found adequate to reproduce the pore pressure buildup aspect, and s standard one dimensional consideration model was used to compute redistribution and dissipation of excess pore pressures.

In the present analysis, the sand layer was divided into eleven horizontal layers with an equal thickness about 55cm. The small-strain shear module G_{max} and the backbone curve of the shear stress versus shear strain relation at the mid heights of the sub-layers were estimated from the upper sand layer data, considering the confining stresses. G_{max} Were shown in Fig. 8. SRANG can consider the degrading of sand shear module in accordance with the increasing of excess pore pressure. Fig. 9 shows the liquefaction characteristics of the test sand, which were obtained the tri-axial cyclic test and computations. The numerical method used to obtain the response of the model pile-foundation system was based on a beam-on-Winkler foundation model. A pile-supported structure was represented by a single-pile system; the structural model was represented by a lumped mass; the pile was divided into eleven equal segments, with each segment being connected to the free-field soil through nonlinear soil-pile elements. The numerical method can account for the effects of 1) nonlinear stress-strain behavior of soil around a pile, and 2) excess pore pressure buildup and dissipation in the free-field and around a pile in both the radial direction away from the pile and the vertical direction.

5 RESULTS FROM NUMERICAL ANALYSIS

Fig. 10 shows the maximum acceleration distributions in depth. The disagreements between test data and computations was found in shallow area. If SRANG will consider the dilatancy, good agreements would be obtained. Fig. 11 shows the acceleration response spectra on free sand surface. Test data gave high responses in comparison with computation. Fig. 12 is the depth distributions of absolute maximum accelerations of piles. Fig. 13 is the depth distributions of absolute maximum strains of pile steel bars. The value of test data shows larger than computations

6 CONCLUSIONS

Experimental data concerning the process of damage and failure of the test piles during liquefaction were obtained. Results were used to improve numerical modeling of soil-pile -structure systems in liquefying sand, and experimental data were compared with computations. This study suggested that the numerical estimation of damage to pile foundation due to liquefaction of soils is reasonable. However, some improvements would be necessary.

ACKNOWLEDGEMENTS

This study was conducted under the committee of EDUS project; Chairman Professor Kenji Ishihara of Tokyo Science University. The authors show special thanks to Mr. Kazuo Sakai, the director of Kiso-Jiban Consultants Co.

REFERENCES

1. Kagawa, T. 1992. Effects of Liquefaction on Lateral Pile Responses. ASCE Geotechnical Special Publication, 34;207-227
2. Kagawa, T., Minowa, C. 1994. Effects of liquefaction on soil-pile-structure interaction. 10th European Conference on Earthquake Engineering, Proceedings 617-622

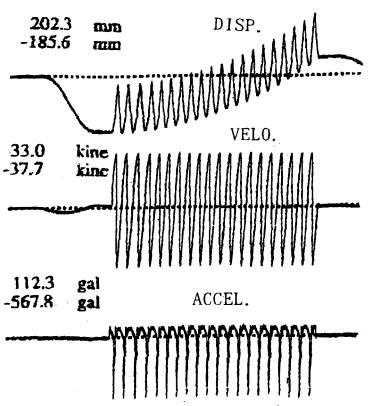

Fig.1 Shaking table movements for residual deformation tests

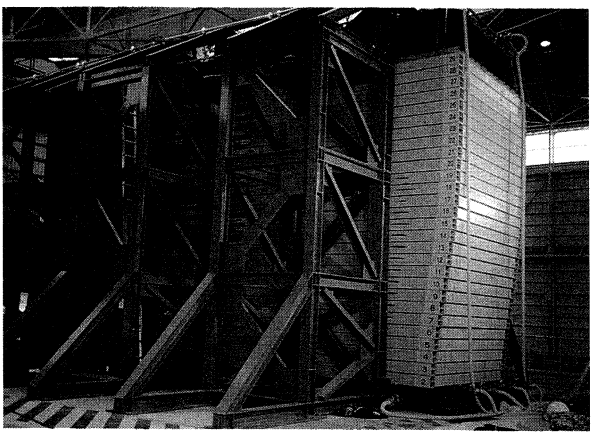

Fig.2 Residual deformation of large-scale laminar shear box.

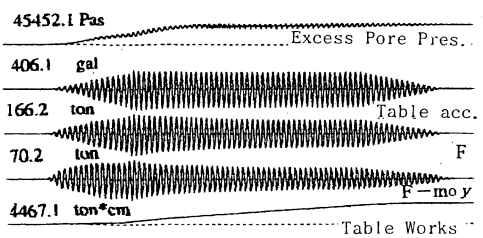

Fig.3 Sinusoidal case of excess pore pressures and shaking table works

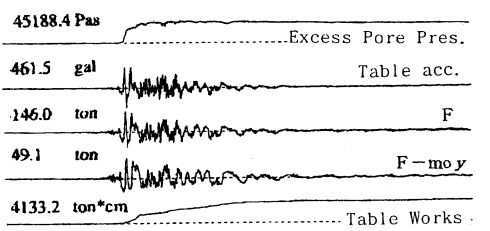

Fig.4 Random wave case of excess pore pressures and shaking table works

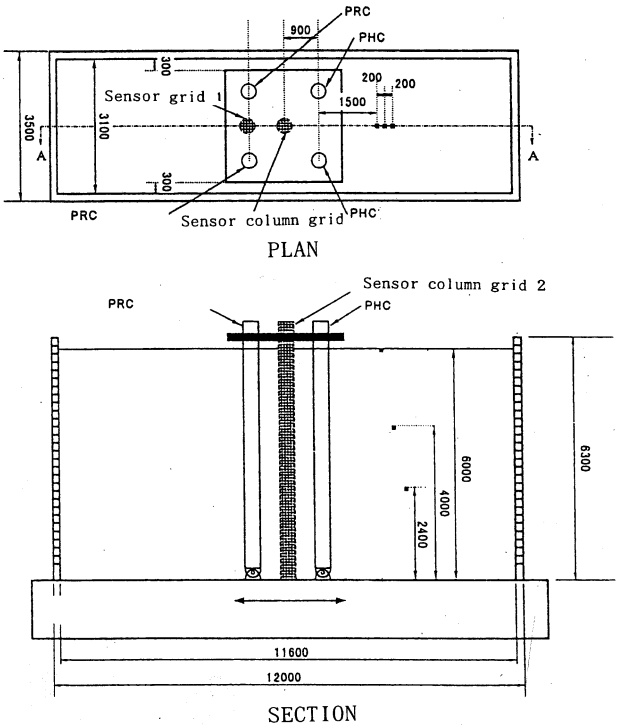

Fig.5 Outline of large-scale laminar shear box and test pile foundation system

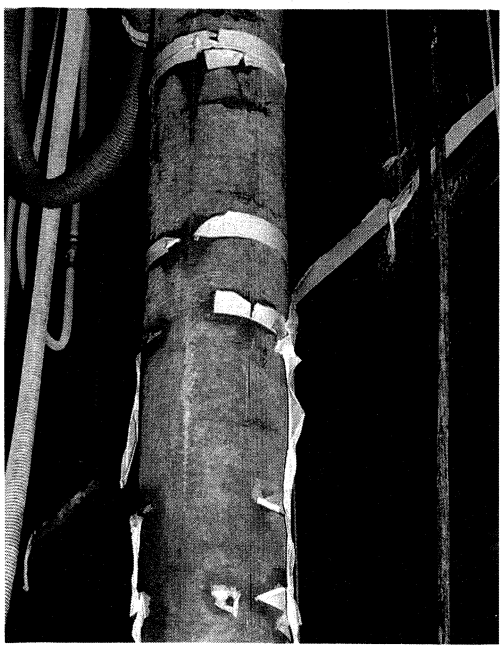

Fig.6 Cracked pile in shear box.

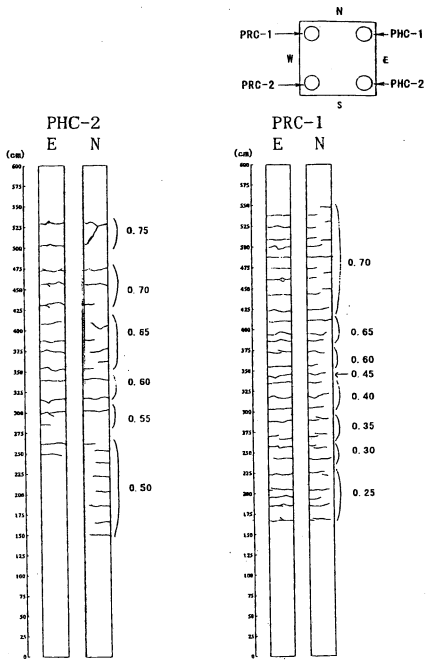

Fig.7 Sketches of pile cracks.

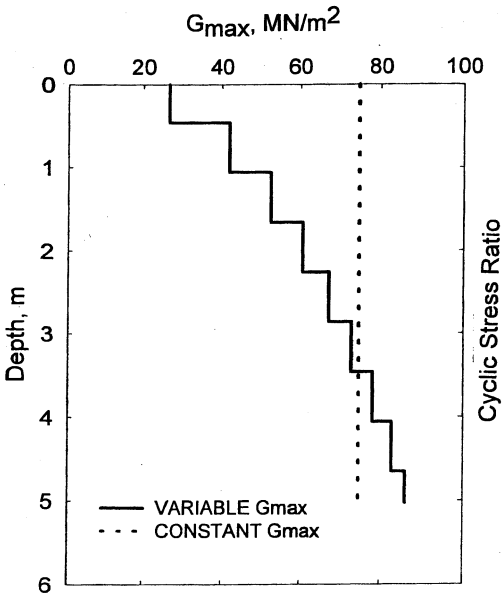

Fig.8 Estimated shear module of test sand layer

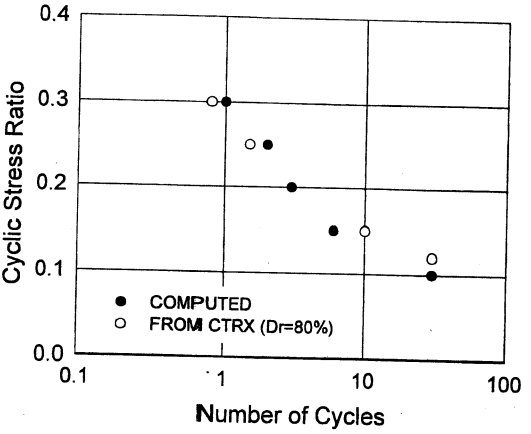

Fig.9 Liquefying characteristics of test sand.

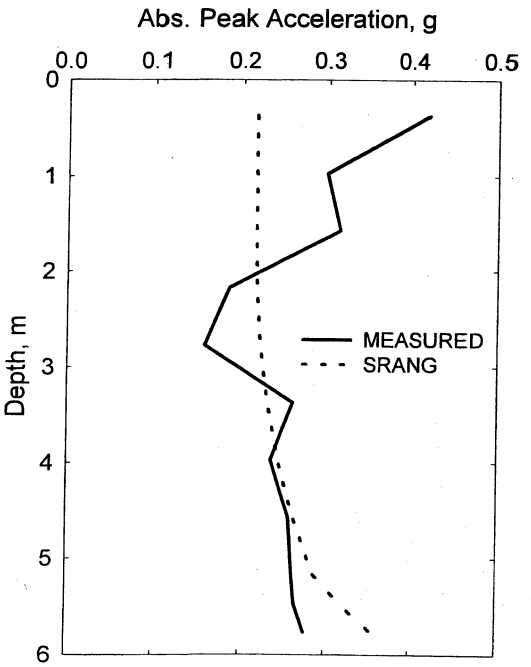

Fig.10 Comparison of sand accel. depth distributions of test and computation

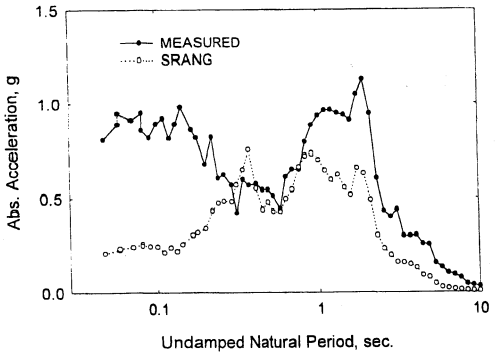

Fig.11 Acceleration response spectra of free sand surface records.

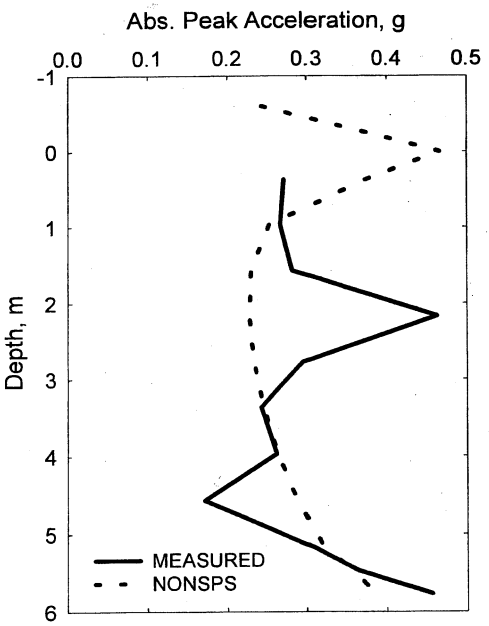

Fig.12 Comparison of pile accel. depth distributions of test and computation

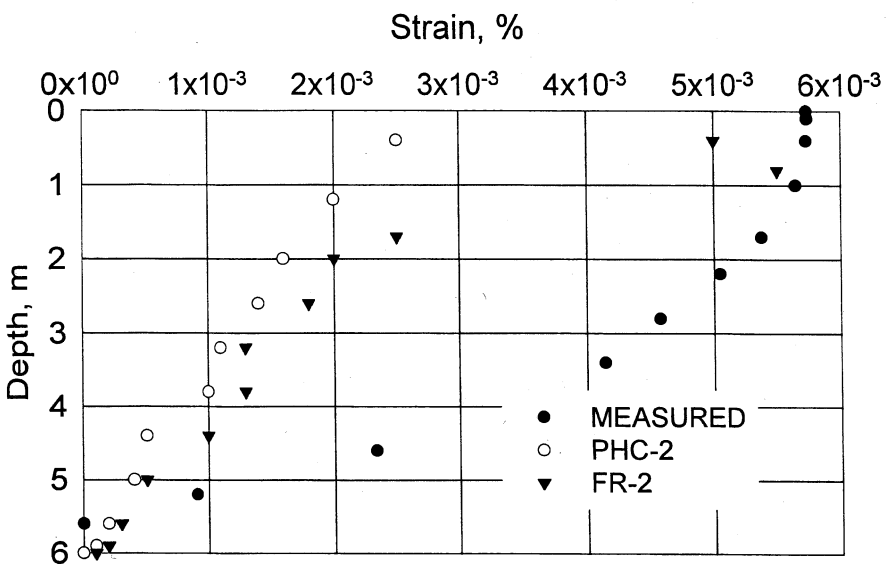

Fig.13 Pile strain depth distribution of test and computation

earthquake and the relative density as indicated in Fig.16.

In the present study, the maximum shear strain (1.5 times of half of the maximum double amplitude axial strain) in the final stage of the liquefaction test and the volumetric strain due to the consolidation after liquefaction were obtained. The test results are also plotted in Fig.16. As shown in Fig.16, the present test results for upper and lower layers are almost distributed on two lines proposed for the sand by Ishihara and Yoshimine with relative densities of 70 % and 90 %, respectively, though the data has some scatters. Test results show a correlation, in which the post liquefaction volumetric strain increases with the increase in the maximum shear strain to about 5% of γ_{max}.

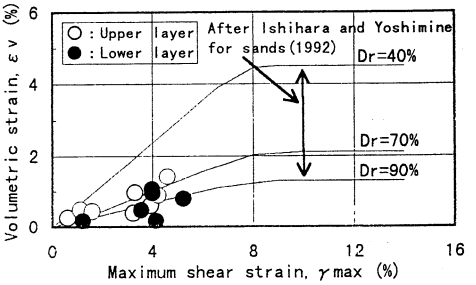

Fig.16 Relations between maximum shear strain and post liquefaction volumetric strain for undisturbed gravel samples

CONCLUSIONS

Based on the laboratory tests for high-quality undisturbed gravelly samples obtained by the in-situ freezing method, following were concluded.

(1) The permeability coefficient of undisturbed gravels is between 7.8×10^{-4} and 10^{-2} cm /sec, these results mean that it is reasonable to assume an undrained condition for the gravel to be subjected to cyclic shear, during earthquake motions.

(2) The undrained cyclic shear strength of the lower gravelly layer is much larger than that of the upper layer. These results are almost coincides with the empirical correlations between Vs and undrained cyclic shear strength proposed by Hatanaka et al (1996).

(3) There can be seen a good empirical correlation between undrained cyclic shear strength and N_{L1} for gravel.

(4) Though the data is limited and has some scatters, there are correlations between the γ_{max} and the post-liquefaction volumetric strain for both gravel samples.

ACKNOWLEDGEMENT

This paper described a part of the "Study on the siting technology of nuclear power plants on Quaternary deposits" by Nuclear Power Engineering Corporation (NUPEC), under the sponsorships of Ministry of International Trading and Industry (MITI) of Japan. The sponsorships and efforts made by all the members of this study are greatly appreciated. In-situ freezing sampling was performed by Tokyo Soil Research Co. Ltd.

REFERENCES

1. Hatanaka,M., Suzuki,Y., Kawasaki,T. and Endo,M. (1988): "Cyclic undrained shear properties of high quality undisturbed Tokyo gravel," Soils and Foundations, Vol.28, No.4, pp.57-68.
2. Hatanaka,M., Uchida,A. and Suzuki,Y. (1996): "Correlation between undrained cyclic shear strength and shear wave velocity for gravely soils," Soils and Foundations. (accepted for publication)
3. Ishihara, K. and Yoshimine, M. (1992): "Evaluation of settlements in sand deposits following liquefaction during earthquake," Soils and Foundations, Vol.32, No.1, pp.173-188.
4. Suzuki,Y., Goto,S., Hatanaka,M and Tokimatsu,K. (1993): "Correlation between strengths and penetration resistances for gravelly soils," Soils and Foundations, Vol.33, No.1, pp. 92-101.
5. Suzuki,Y., Hatanaka,M., Konno,T., Ishihara,K. and Akino, K.(1992): "Engineering properties of undisturbed gravel samples, "Proc. of 10th World Conference on Earthquake Engineering, Madrid, Vol.3, pp.1281-1286.

these samples are replotted in Fig.13 for comparisons. As indicated in Fig.13, the stress ratios for DA=2% in 20 cycles are 0.40 (upper layer) and 0.69 (lower layer), respectively.

The liquefaction strength for undisturbed gravel samples obtained in the present study used for investigating the correlation between N_{L1} and cyclic undrained strength for high-quality undisturbed gravel as shown in Fig.14. The data obtained by Suzuki,Y. et al (1993) was also used for this study. It is obvious that there is a fairly good correlation between $R_{N=15}$ and the N_{L1}. The N_{L1} value is a LPT N-value normalized at the effective overburden pressure of 98 kPa by using Eq. (5).

$$N_{L1} = N_L(98/\sigma_v')^{0.5} \qquad (5)$$

where, σ_v '(in kPa) is the effective overburden pressure at the depth where LPT was performed.

Fig.15 shows the empirical correlation (Eq.(6)) between shear wave velocity (Vs) and undrained cyclic shear strength at 15 cycles of cyclic shear ($R_{N=15}$) proposed by Hatanaka et al (1996). The test results obtained in the present study are also plotted in Fig.15 as solid triangles. There can be seen fairly good agreement between the present test results and the proposed correlation. These results suggest that the in-situ Vs is a useful parameter for estimating the undrained cyclic shear strength of in-situ gravelly soils.

$$R_{N=15} = 0.082 + 9.5\times10^{-4}V_{S1} \qquad (6)$$

$$V_{S1} = V_S/(\sigma_v'/98)^{1/4},\ \sigma v': \text{kPa} \qquad (7)$$

Post liquefaction volumetric strain

Estimation of the post liquefaction volumetric strain of the foundation soils is one of the most important tasks for foundation designs. Ishihara and Yoshimine (1992) proposed a simple method for estimating the post liquefaction volumetric strain of saturated sand based on the laboratory test results for sand. In the simplified method, the post liquefaction volumetric strain is related to the maximum shear strain induced during an

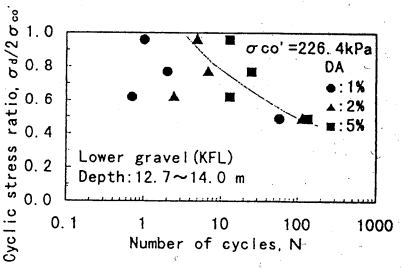

Fig.12 Undrained cyclic shear strength test results for lower gravel (KFL)

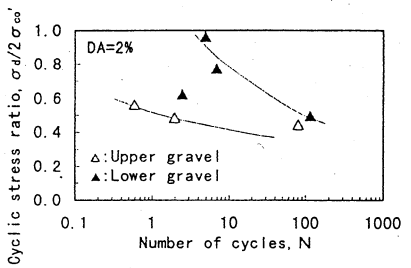

Fig.13 Cyclic stress ratio required to cause DA=2 % for undisturbed gravel samples

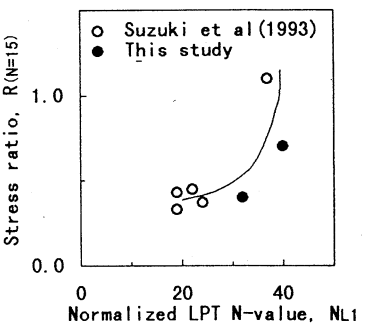

Fig.14 Relationship between R_N=15 and N_{L1} for gravels

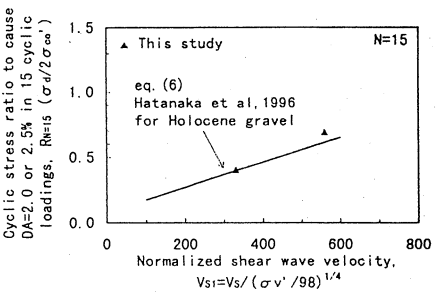

Fig.15 Vs－$R_{N=15}$ relation for gravels

3) After the specimen has been thawed completely, it is saturated with the aid of CO_2 gas, the deaired water and a back pressure of about 196 kPa (2.0 kgf/cm^2), until the pore water pressure coefficient B-value reaches 0.95 or higher. After saturation, the specimen is isotropically consolidated at a specified confining pressure, which is equal to the effective vertical stress at the sampling depth.
4) After consolidation, cyclic deviator stresses are applied to the specimen in an undrained condition.
5) After the undrained cyclic shear, the specimen is returned to the drained state, and the volume change due to the consolidation, is measured.

In the present study, steps 1) to 4) are the "undrained cyclic shear test" which measures the liquefaction strength, while step 5) is performed in order to determine the volumetric strain induced by the undrained cyclic shear.

Cyclic undrained triaxial test results

The physical properties of undisturbed gravel samples used in cyclic undrained triaxial tests are described in Table 3. Figure 9 indicates the typical time histories of the cyclic deviator stress, excess pore water pressure and axial displacement during the cyclic undrained triaxial tests for undisturbed samples obtained from the upper gravelly layers (KFU sample). It can be seen that the amplitude of the cyclic deviator stress was successfully maintained at a constant level, even when the specimen deformed with more than 5 % of double amplitude axial strain (DA). Fig.10(a) shows a typical stress-strain relationship of undisturbed gravel sample during the cyclic shear. It is clearly seen that the axial strain progresses on the extension side, gradually. Fig.10(b) displays a typical stress path of the undisturbed sample.

The correlations between the cyclic stress ratios required to cause a double amplitude axial strain (DA) of 1, 2 and 5 % and the cycles of stress application are indicated in Figs.11 and 12 for the KFU and KFL samples, respectively.

The stress ratios to cause DA=2 % for

Table 3 Physical properties of gravel samples used in cyclic undrained shear test

Sample name		50% diameter (mm)	Maximum diameter (mm)	Fines content (%)	Dry density (g/cm^3)	Particle density (g/cm^3)	Uniformity coefficient, Uc
KFU	C-2-1	32.2	125	0.5	2.105	2.68	54.3
	C-2-2	36.3	125	0.3	2.253	2.69	79.3
	D-2-1	27.9	125	0.3	2.237	2.72	50.4
	D-2-2	36.7	125	0.5	2.167	2.67	63.3
KFL	C-6-1	19.1	125	0.6	2.233	2.68	43.0
	C-6-2	19.8	106	0.4	2.181	2.69	40.4
	D-6-1	14.1	106	0.5	2.159	2.68	44.1
	D-6-2	12.2	125	0.3	2.144	2.69	30.7

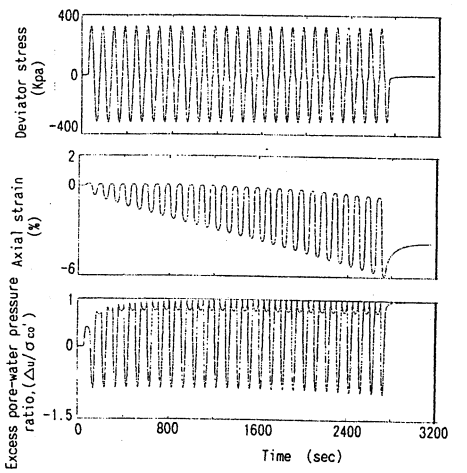

Fig.9 Typical time histories of undrained cyclic shear test

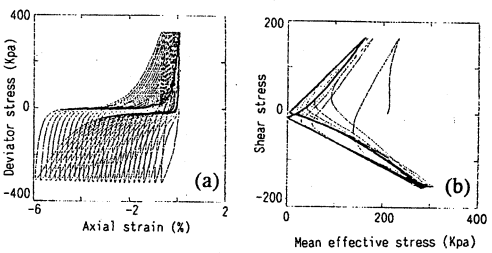

Fig.10 Typical stress-strain relationships (a) and stress paths (b) during undrained cyclic shear

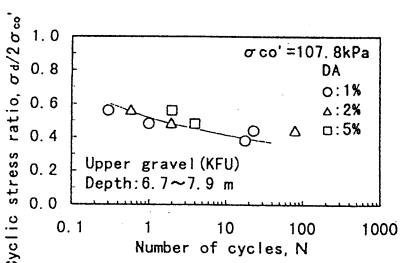

Fig.11 Undrained cyclic shear strength test results for upper gravel (KFU)

ficient for gravely soils. Figure 7 indicates the comparison of permeability coefficient between test results and Creagar's proposal. It is obviously that Creagar's proposal also overestimates the in-situ permeability coefficient of gravely soils. Based on the test results, it is reasonable to assume the undrained condition for cyclic shear, during earthquakes for the present gravel.

APPARATUS AND PROCEDURES FOR UNDRAINED CYCLIC SHEAR TESTS

Large Scale Cyclic Triaxial Test Apparatus

The test apparatus used for the determination of the undrained cyclic shear strength of undisturbed gravel samples is schematically shown in Fig.8. The confining stress was applied pneumatically while the cyclic load was applied by hydraulic pressure. The load transducer was placed inside the cell to determine the axial load accurately. The axial displacement of the large strain level near the liquefaction was monitored by a linear variable differential transducer (LVDT) mounted on the loading rod. The cyclic deviator stresses were applied in uniform sinusoidal cycles at a frequency of 0.01 Hz. The low frequency was selected in order to maintain the constant amplitude of the cyclic deviator stress even at a large amount of the axial strain. The electrical output from the load cell, displacement transducer, and pore water pressure transducer was amplified and then simultaneously recorded on a floppy disc for a desk top computer.

Testing Method

The procedures of the cyclic undrained triaxial tests were as follows:

1) The frozen test specimen (diameter: 30 cm, height: 60 cm) is placed on the pedestal, and is then covered with a rubber membrane and sealed to the pedestal and top cap using O-rings.

2) The frozen specimen is then allowed to thaw in a drainable state under a confining stress of 19.6 kPa at room temperature.

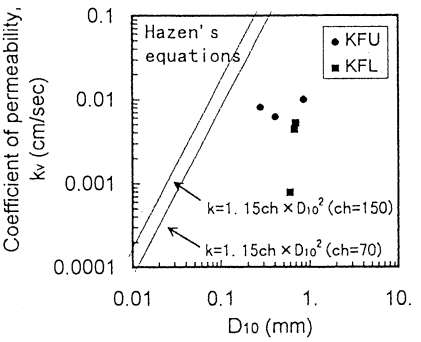

Fig.6 Comparison of test results with Hazen's equations

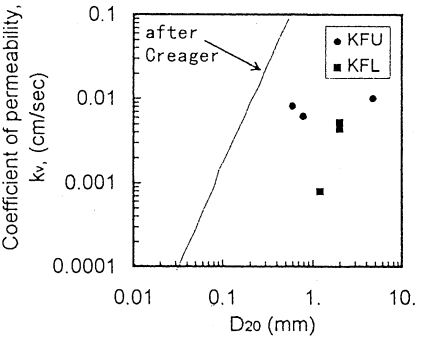

Fig.7 Comparison of test results with Creagar's proposal

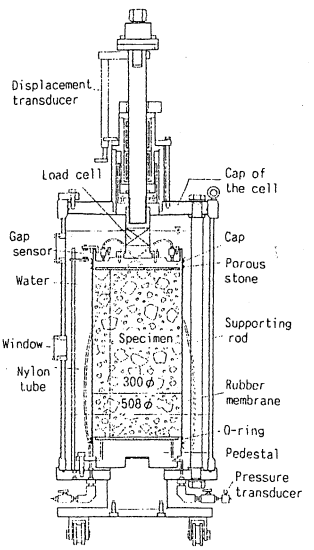

Fig.8 Schematic diagram for the cell of large-scale triaxial test apparatus

under a small confining stress in the drained condition. After the specimen has thawed completely, it is saturated with the aid of CO_2 gas , the de-aired water and a back pressure of about 1.0 to 2.0 kgf/cm^2 (98 to 196 kPa), until the pore pressure coefficient B-value reaches 0.95 or higher.

④ After saturation, a specific confining pressure is applied by air pressure through a water medium for consolidation. After consolidation, the de-aired water is allowed to flow through the specimen from burette A to burrete B for measuring the permeability coefficient.

The initial all-around confining stress used in the permeability tests are as σ_v', $0.5\,\sigma_v'$ and $2.0\,\sigma_v'$, where σ_v' is the effective vertical stress at the sampling depth. The permeability test starts from the lowest confining pressure, and at each step of confining stress, the test starts from the lowest hydraulic gradient of 0.1 and enlarges its value at an interval of 0.1 to the maximum value of 0.5.

Test results

Figure 5 indicates the typical test results of the permeability coefficient (Kv) of undisturbed gravel samples. The coefficient of permeability at i=0.3 is summarized in Table 2 with their physical properties. The following results can be pointed out.

① The permeability coefficient of both upper and lower gravel samples is between 7.8×10^{-4} and 1×10^{-2} cm/sec, the lower gravelly layer indicates slightly lower permeability.

② There can be seen a trend that the coefficient of permeability decreases with increasing confining stress, and this is thought to occur due to the slight decrease of the void ratio of the sample with increasing confining stress.

③ The permeability coefficient of gravel samples is almost unchanged in the range of the hydraulic gradient larger than i=0.3.

Figure 6 shows the comparison of test results with Hazen's equations as a function of 10 % diameter (D_{10}). Test results indicate that Hazen's equations much more overestimate the permeability coef-

Photo 2 Frozen gravel sample (30cm ϕ × 60cmH)

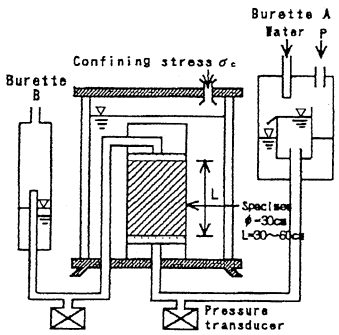

Fig.4 Schematic diagram of permeability test apparatus for gravel samples

Table 2 Permeability test result and physical properties of gravel samples tested

Sample name		10% diameter (mm)	20% diameter (mm)	Fines content (%)	Dry density (g/cm^3)	Particle density (g/cm^3)	Permeability coefficient, Kv (cm/s) i=0.3, $\sigma_v'=\sigma_v'$
KFU	A-3-1	0.28	0.6	0.6	2.016	2.70	8.1×10^{-3}
	B-2-1	0.86	4.7	0.2	2.121	2.71	1.0×10^{-2}
	D-3-1	0.41	0.79	0.6	1.989	2.70	6.2×10^{-3}
KFL	A-7-1	0.70	2.0	0.3	2.094	2.72	5.2×10^{-3}
	B-3-4	0.67	2.0	0.2	2.240	2.71	4.4×10^{-3}
	B-4-2	0.60	1.2	0.4	1.997	2.69	7.8×10^{-4}

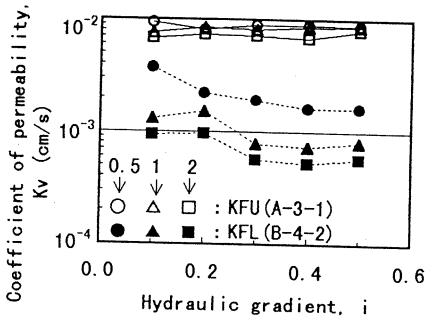

Fig.5 Typical permeability test results

118cm in diameter is then placed into the hole to prevent any collapsing. Five guide pipes fixed by two steel plates at both ends shown in Fig.3, were installed into the bottom of the 120 cm hole in order to exactly determine the locations of the freezing pipe (one 164 mm-pipe) and sampling places (four 406 mm-pipes).

② A 76 mm bore hole is drilled to a depth slightly lower than the sampling depth with extreme care. An outer freezing pipe (73 mm in diameter) with a PVC rod at the tip is carefully installed into the 76 mm hole. A series of thermocouples is set on the PVC rod for monitoring the ground temperature during freezing.

③ A 22 mm diameter inner pipe with an open-end is then placed into the 73 mm pipe with about a 100 mm clearance from the bottom. Liquid nitrogen is fed into the inner pipe to freeze the surrounding ground. After about a 4 days supply of liquid nitrogen, about a 120 cm diameter frozen gravel column can be achieved.

④ The undisturbed gravel samples are recovered from an undisturbed area about a diameter from the outside of the cylindrical surface of the outer pipe. Chilled mud is used in coring the frozen gravel, for keeping the frozen sample from thawing during coring.

⑤ The frozen gravel column is separated at the lower end of the sampler, about one m long, by pulling the double tube core barrel using a boring machine.

⑥ The frozen gravel column is pulled out of the double tube core barrel after the tube has been lifted up to ground level. Photo 1 shows the frozen gravel column just extracted from the double-tube core barrel.

⑦ The frozen gravel column is then cut to a length of 60 cm in the sampling site using a special diamond saw for preparing a test specimen used in the large-scale triaxial test apparatus. Photo 2 shows the frozen gravel sample prepared in the field.

LABORATORY PERMEABILITY TESTS ON HIGH-QUALITY UNDISTURBED GRAVEL SAMPLES

In the present study, the cyclic shear strength and the induced post cyclic shear volumetric strain behavior of gravels are discussed based on the assumption of an undrained condition during earthquakes. In order to verify this assumption, it is important to investigate the permeability coefficient of in-situ gravelly soils.

For this purpose, the permeability coefficient of undisturbed gravel samples both of upper and lower layers were measured in laboratory tests.

Testing apparatus and testing method

A schematic diagram of the permeability testing apparatus using a triaxial cell is illustrated in Fig.4. With this testing system, a constant-head type permeability test can be carried out for a specimen at an isotropic confining stress.

The test procedures are as follows.

① A test specimen was placed between two porous plates which enable the free drainage of the water during consolidation and permeability tests.

② The specimen is then covered with a waterproof rubber membrane. The rubber membrane is sealed from the top cap to the pedestal using O-rings. The top and bottom of the specimen are connected to burette B and burrete A, respectively.

③ The frozen specimen is then thawed

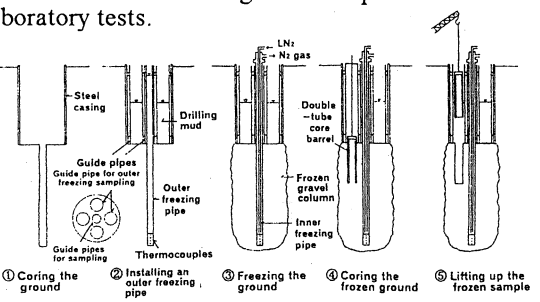

Fig.3 Procedure of in-situ freezing sampling method

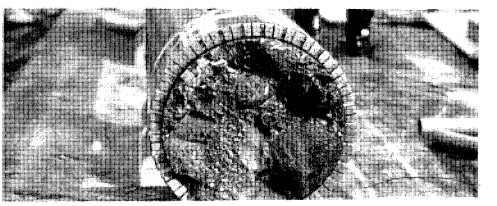

Photo 1 Frozen gravel column cored in the tube